A Passive Battery Management System for Lead-Acid battery

Adrian Augustin POP
Dpt. of Electrical Machines and Drives
Technical University of Cluj-Napoca
Strada Memorandumului 28, Cluj-Napoca 400114, Romania
Augustin.Pop@emd.utcluj.ro

Razvan INTE
Dpt. of Electrical Machines and Drives
Technical University of Cluj-Napoca
Cluj Napoca, Romania
Razvan.Inte@mae.utcluj.ro

Claudiu OPREA
Dpt. of Electrical Machines and Drives
Technical University of Cluj-Napoca
Cluj Napoca, Romania
Claudiu.Oprea@emd.utcluj.ro

Mircea RUBA
Dpt. of Electrical Machines and Drives
Technical University of Cluj-Napoca
Cluj Napoca, Romania
Mircea.Ruba@emd.utcluj.ro

***Abstract*— One of the dangerous issues that can appear when working with batteries is the imbalance of the cell. To overcome this problem, the battery management systems (BMS) can provide balancing by extracting or adding charge according to the needs. The goal is to protect the battery from dangerous overheating or damage but also to prolong the battery's lifetime. Without a BMS the individual cell voltage will drift away, and the estimation of the state of charge will be unreal. The BMS is detecting automatically when the battery pack is charged, and it enables passive balancing of charged cells. The goal of this paper is to test the BMS system adapted for lead acid batteries and visualizing the performances by using real time application by means of graphical instruments. The measured parameters as current, voltage, temperature is displayed with the help of dSPACE and Typhon HIL platforms.**

Keywords: battery cell, balancing, battery management system

I. INTRODUCTION

A Battery Management System (BMS) is a critical component designed to ensure the safe, reliable, and cost-effective operation of battery systems. Its primary function is to maintain uniform energy distribution across all cells within the battery pack, thereby enhancing overall performance and longevity. In addition to its hardware architecture, a BMS requires the integration of advanced software algorithms capable of accurately measuring and estimating key battery parameters such as the State of Charge (SOC), State of Health (SOH), and Remaining Useful Life (RUL).

The software must also implement protective functions to guard against hazardous conditions including overcharging, thermal runaway, and deep discharge, ensuring each cell operates within its designated Safe Operating Area (SOA). One of the common operational challenges arises from voltage imbalances among cells connected in series, which may result from disparities in SOC, internal impedance, or cell capacity.

A significant differentiation between lithium iron phosphate ($LiFePO_4$) and lead-acid batteries lies in their response to discharge rates. Specifically, $LiFePO_4$ batteries exhibit minimal capacity degradation under high discharge rates, unlike lead-acid batteries, which experience a marked reduction in usable capacity. As illustrated in Figure 1, when subjected to an 8C discharge rate, the effective capacity of a lead-acid battery drops to approximately 60% of its nominal rating, as depicted in Figure 2.

Additionally, low ambient temperatures adversely affect the capacity of all battery chemistries. Two critical factors must be considered under these conditions: charging and discharging performance. Lithium-based batteries exhibit poor charging acceptance below 0 °C, often requiring thermal conditioning. Conversely, lead-acid batteries can tolerate limited charging currents even at sub-zero temperatures.

Given the operational requirement to employ lead-acid batteries—specifically at a 12 V nominal voltage level—this study focuses on the design and implementation of a dedicated BMS architecture tailored for lead-acid chemistry, addressing the unique challenges associated with temperature sensitivity, charge acceptance, and cell balancing.

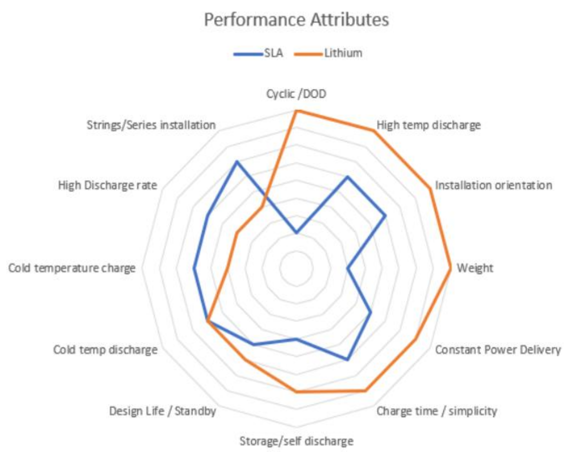

Fig.1. Comparison between lithium and lead acid batteries

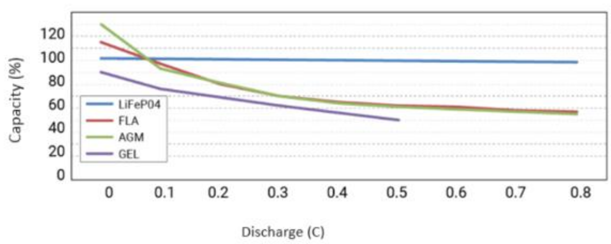

Fig.2. The capacity of different lead acid batteries vs lithium battery

Cell balancing techniques are generally categorized into active and passive methods. The fundamental distinction between these approaches lies in the way energy is redistributed among the battery cells. In active balancing, excess energy from higher-charged cells is transferred to lower-charged (weaker) cells using energy storage elements such as inductors, capacitors, or transformers. In contrast, passive balancing dissipates the surplus energy of the most charged cells as heat through electronically controlled resistive paths, typically using switchable resistors.

Passive cell balancing is widely adopted due to its simplicity, low implementation cost, reliability, and ease of integration. While active balancing circuits are capable of handling current levels in the order of several hundred amperes, passive balancing systems are typically limited to current levels in the hundreds of milliamps range. Passive balancing is also commonly referred to as "resistor bleeding" or dissipative balancing. Its operating principle involves discharging overcharged cells via a parallel resistive load, effectively bypassing the main discharge path. A notable drawback of this method is that the energy imbalance is irreversibly lost as thermal energy, which reduces overall system efficiency. Despite this limitation, passive balancing is also employed during the discharge cycle to maintain cell voltage uniformity.

For battery chemistries such as lead-acid and nickel-based cells, passive balancing is typically sufficient. These chemistries are inherently more tolerant to overcharge conditions, making the simpler resistive balancing approach both effective and safe.

A basic implementation of passive balancing involves a dissipative resistor-based circuit, as illustrated in Figure 3, where each cell is equipped with a bypass resistor and a control switch to selectively bleed off excess charge.

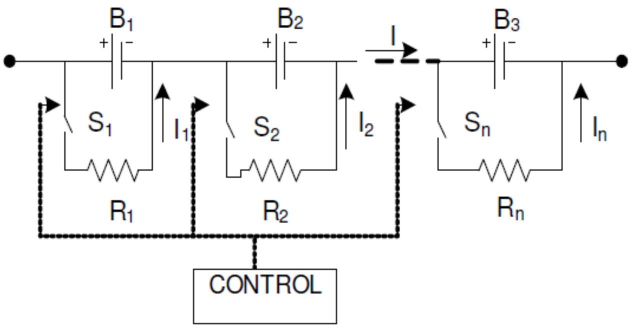

Fig.3. Dissipative resistor balancing circuit

The system under consideration is capable of operating in two distinct modes: continuous mode and detection mode. In continuous mode, all relays are simultaneously actuated by a common control signal—either in the ON or OFF state. This configuration is primarily utilized during the charging phase, wherein the cell with the higher terminal voltage naturally draws less current, due to the voltage drop across the balancing resistor. When the resistor value is appropriately selected, this method enables a simple yet effective passive balancing mechanism. Its primary advantage lies in its lack of need for complex control logic, simplifying both design and implementation.

In detection mode, a microcontroller-based control unit is employed to monitor individual cell voltages, detect imbalances, and activate the dissipative resistors only when necessary. This conditional control strategy enhances efficiency by engaging balancing only when an overvoltage condition is detected on a particular cell.

The balancing circuit implemented in this study consists of two identical branches, each composed of a power resistor and a Darlington transistor, as illustrated in Figure 4. Each branch is designed to divert a portion of the charging current away from overcharged cells. The low-resistance power resistors facilitate rapid energy dissipation, while the Darlington transistor configuration permits control over relatively large current levels, thereby contributing to a reduction in overall charging time. To mitigate thermal buildup, an aluminum heat sink is installed beneath the power transistors to ensure adequate thermal dissipation.

In the subsequent section, two commercially available battery balancers are evaluated. For confidentiality and comparative analysis, they are referred to as Battery Balancer 1 and Battery Balancer 2.

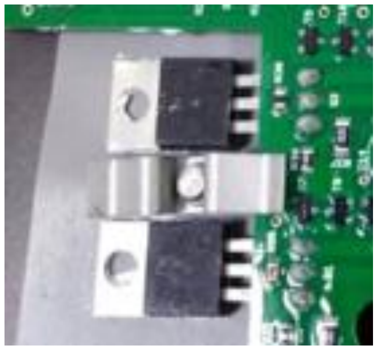

Fig.4. Dissipative resistor balancing circuit

To validate the electric power storage and supply system of the hybrid funicular, we began by simulating the entire system using the Simcenter Amesim software, allowing us to visualize the results for each individual subsystem or component. Since the system is complex the command was simplified and run only specific cases that are according to the client requirements. Figure 5 illustrates the prototype of the electric funicular. Before assembly onto the prototype, the subassemblies of the funicular are tested independently to ensure their functionality. To evaluate the performance of the energy storage and supply system, we extracted the consumption curves from the model, which will be applied to the constructed experimental setup.

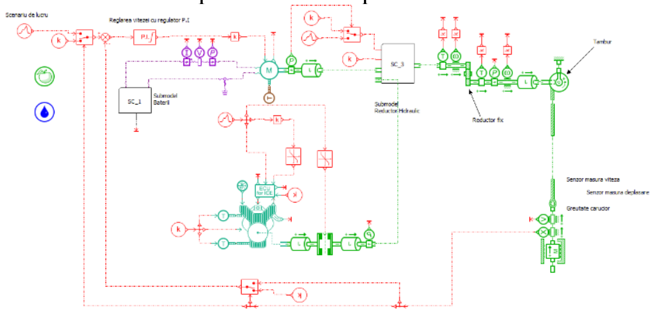

Fig.5. Hybrid forest funicular system schematics.

In Figure 6, we can observe the batteries connected in series, serving as the power source for the entire electric drive system. The series connection of the batteries is designed to increase the voltage level to meet the necessary amplitude for the inverter. The simulation of the storage and supply system was conducted for various scenarios, depending on the operational length of the line and the weight of the timber load. For all simulated cases, the most challenging operational scenario was considered, with an incline of 45 degrees. Simulations were performed for operational line lengths of 500m, 1000m, 1500m, and 2000m.

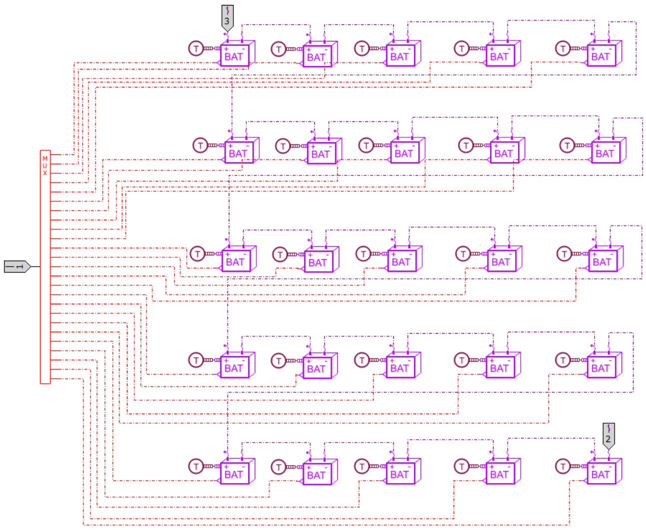

Fig.6. The series batteries connection for the storage/power supply system designed in Amesim

Current curves were extracted from Simcenter Amesim according to the following scenario: the carriage ascends from ground level to 500m, 1000m, 1500m, or 2000m, where it pauses while operators load the timber. The next step involves lifting the timber from the ground, during which the batteries supply the maximum discharge current of 70A. Subsequently, the carriage recovers energy throughout the descent. Once the funicular reaches ground level, it is unloaded, at which point a pause is included in the scenario. This cycle repeats over a duration of 8 hours, which is the typical operating time for the funicular in a day. The scenario was observed during visits to forestry operations.

For the operational scenarios, the ascent speed of the carriage is limited to managing the current draw from the batteries. It can be noted that as the length of the funicular operation increases, so does the ascent time. The following figures depict the four current curves extracted from Amesim for the predefined working scenario. In Figure 7, the scenario for the funicular operating on a 500m line shows a total duration of approximately 23 minutes. For the case where the funicular operates over a length of 1000m, a complete scenario lasts about 32 minutes, as illustrated in Figure 8, Figure 9-1500m and Figure 10-2000 m.

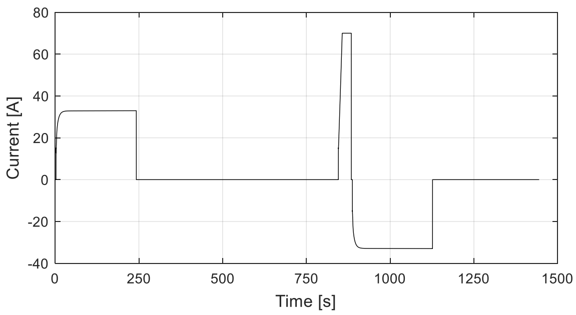

Fig.7. Current curve for a working funicular line length of 500m

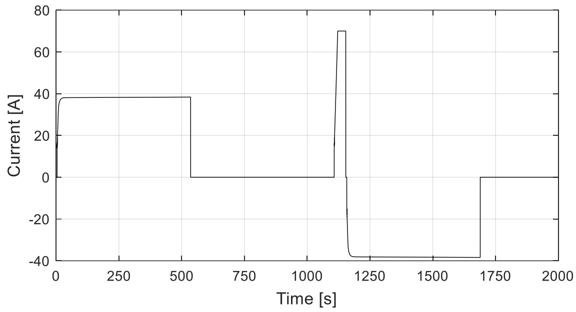

Fig.8. Current curve for a working funicular line length of 1000m

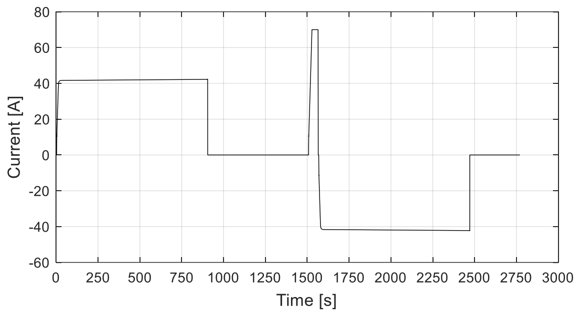

Fig.9. Current curve for a working funicular line length of 1500m

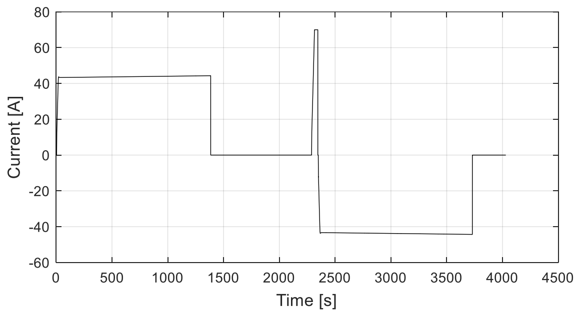

Fig.10. Current curve for a working funicular line length of 2000m

This comprehensive analysis provides valuable insights into the performance and efficiency of the funicular's electric power storage and supply system.

II. TESTING THE BATTERY BALANCER 1

The energy storage system for the hybrid forest funicular consists of 24 AGM-VRLA Lead Acid Batteries connected in series [2-3]. Due to the limitation of the power source and electronic load available in the laboratory the test can be made only for 6 AGM-VRLA batteries connected in series. To test the power system of the hybrid funicular, a test bench consisting of 6 AGM-VRLA Lead Acid cells (batteries) connected in series was made. The implemented system is designed for six lead acid batteries cells connected in series, with a pack nominal voltage of 12 V.

During these work stages, a series of measurements were made on a group of six batteries used in the battery bank. Thus, measurements were carried out both in the situation of discharging the group of six batteries and in the situation of charging them.

II.1 Real time batteries testing using dSPACE platform

In Fig. 11 the experimental test bench developed for the battery tests is presented. It consists of the battery system, the battery balancing systems, the differential voltage probes, the dSPACE platform, the DC power supply and the dc programable dc load.

Fig.11. The balancing and measurement system

As far as the batteries are concerned, there are 6 of them connected in series and 5 balancing systems are used. To test the proper functioning of the balancing system, a series of measurements were made both by direct method using classical multimeters and by using differential voltage probes. The differential voltage probes are connected to the dSPACE platform on analogue inputs and data acquisition is done in real time. Battery Balancer equalizes the state of charge of two connected 12V battery strings, or several parallel connected battery strings.

When the voltage between two batteries rises above 27.3V, the Battery Balancer will switch on and compare the voltage of the two connected battery strings. The Battery Balancer will use up to 1 A current from the battery with the highest voltage. The resulting difference in charge will ensure that all batteries will reach the same state of charge. If necessary, several Battery Balancers can be connected in parallel.

To be able to make measurements on the voltage on each battery a code for analog acquisition has been developed in the Matlab Simulink environment and has been further built to be used in ControlDesk together with dSpace platform. In Figure 12 the 6 channels for voltage measurement are presented together with the current measurement. A variable has also been added for each probe to calibrate them before starting the tests. To set the amplification and attenuation of the probes, a gain block has been introduced.

In Figure 13 shows the real-time data acquisition. The battery voltages vary between 12.2V and 12.6V. When the sum of the voltages between two connected batteries exceeds the threshold of 27.3V the balancing system is activated.

The first tests that are made for constant discharge and charge current of the battery pack to test if the battery balancing circuits are working. In table I, we can see the results after a discharge period of 1 hour at 20A there is present an imbalance about 0.1V, and after the charging period at the same current the discharge is amplified up to 0.2V. This proves that the battery balancers circuit didn't balance the batteries fast enough and if there are multiple cycles run the unbalance will grow.

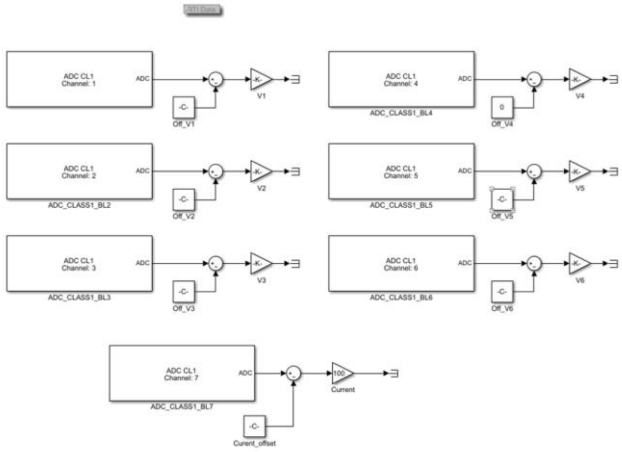

Fig.12. Data acquisition of with the use of Matlab Simulink programming environment and real time dSPACE platform

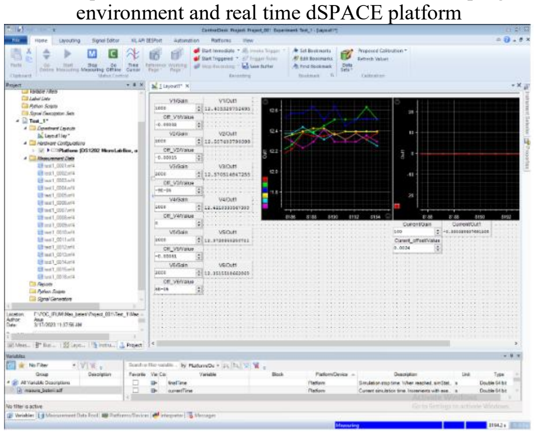

Fig.13. The Control desk interface for controlling the measurements.

TABLE I. MEASURED VALUES

Charging rate	BAT1 (V)	BAT2 (V)	BAT3 (V)	BAT4 (V)	BAT5 (V)	BAT6 (V)
Before discharging	12.96	12.97	12.99	12.95	12.92	13
Discharging 1 hour (20 A)	12.3	12.3	12.32	12.28	12.25	12.33
Charging 1 hour (20 A)-	13.94	13.99	13.97	13.87	13.81	13.94
Charging 1 hour (20 A)- charging completed	13.2	13.15	13.19	13.13	13	13.17

II.2 Real time batteries testing using Typhoon HIL platform

The second test on the batteries was performed with the use of Typhoon HIL 604 programmable control equipment, two power supplies connected in parallel and an electronic load, all controlled by this platform. Figure 6 shows the composition of the test stand. Here it is noticeable the presence of 6 cells, the picture was taken at the end of the tests. After the whole system was installed, voltage measurements were calibrated together with the current sensor. According to the battery characterization and testing procedures, the first step to be performed is cycling and preconditioning [9]. This step is performed at least twice and involves applying a discharge and charge sequence at a current of up to 0.5C. In this case a current of 20A was chosen, representing 0.28C, which is considered sufficient to activate battery chemistry. Figure 8 shows the 2 cycling steps. Figure 14-left, details the first stage, in which it can be seen that, as the battery cells are new they remain in equilibrium throughout the charging process. It takes around 14 hours to achieve the first cycling. At the 2nd stage, the imbalance between cells has already occurred, thus the time of reaching the minimum or maximum allowable cell voltage occurs faster. For this reason, the process was completed after 10 hours.

It should be noted that if the cells are unbalanced, the energy stored in the whole battery is not properly exploited. The protection system is triggered as soon as the most unbalanced cell reaches the thresholds (9V), even if the rest of the cells would still be able to deliver energy. This gave a first indication that the balancing method of the first system is neither efficient nor capable of responding correctly to the requirements of the present system. However, to properly verify the battery balancer 1 solution the tests were continued.

The next step was to carry out a battery discharge at a constant current of 20A by observing the reaction of the cells, Figure 15. The voltage of cell number 1 prematurely reaches the 9V threshold which alarms the protection system and stops the test process. At the same time, to quantify the imbalance, the difference between the voltage of the cell with maximum and minimum load was measured. On the last measurement from Figure 16, this difference can reach beyond 2V which is unacceptable for a power system.

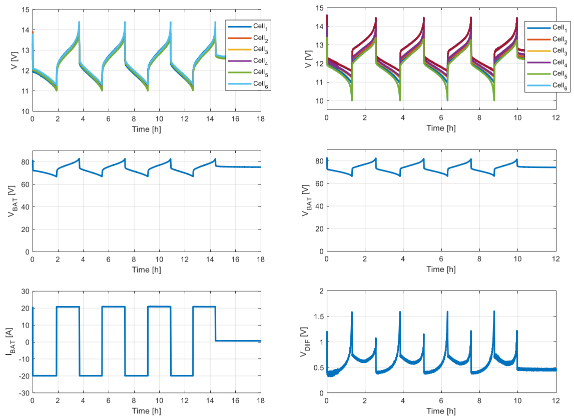

Fig. 14. The two stages of cycling

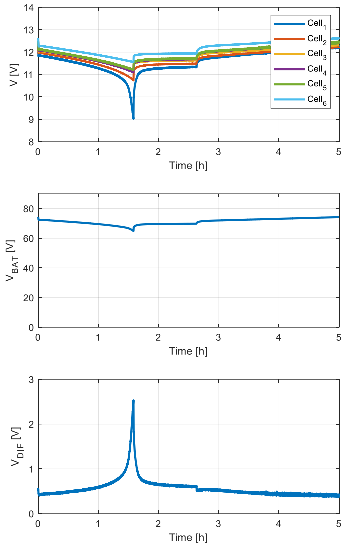

Fig. 15. Discharge test

The tests continued with the application of a running profile for the funicular to a 500m run with and without a break at the arrival of the trolley. It can be seen firstly that power is available for approximately 3 hours of operation without a break and 5 hours with a break, Fig.10. This is due to the strong imbalance that causes the protection system to disconnect the battery when the lower voltage limit of 9V is reached by any of the cells.

In the two tests this difference was measured and in the one without breaking we started from SOC=80% and in the one with break from SOC=100%. When starting from SOC=80%, the imbalance is already stronger, and it becomes more pronounced as the battery discharges. It should be noted that the first system has a balancing current of barely 0.7A only when SOC is close to 100%.

It must be noted that the SOC estimation is based on the Coulomb counting method, that relies on the measurement of the current (Ibat) and its integration on the step time (Δt) considering the actual battery capacity (Q), as detailed in (1). [4 - 8]

$$SOC = \int \frac{I_{bat}}{Q} dt$$
$$SOC(t) = SOC(t-1) + \frac{I_{bat}}{Q} \Delta t \quad (1)$$

Noting that the unbalance cannot be handled by the first system, the tests were discontinued for safety reasons, as the difference in cell voltage increased with each test. Thus, the first system was totally invalidated, and an alternative solution was considered to solve this problem.

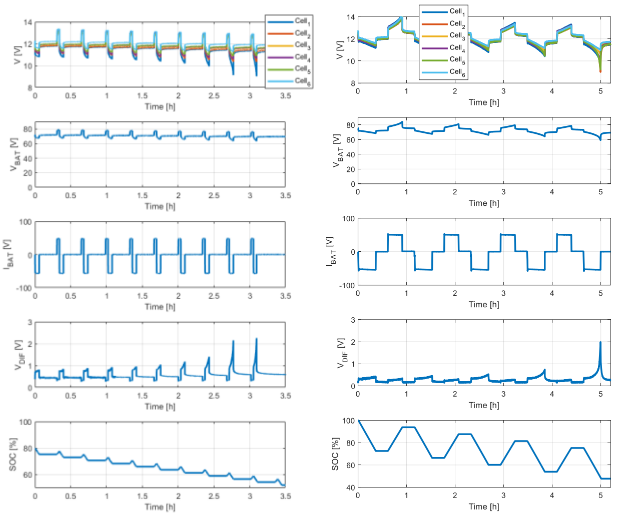

Fig. 16. Funicular running scenarios: route length 500m, profile without break (left) and with break (right) on arrival

As a conclusion this system is only functional under precisely defined conditions, i.e. when the batteries are almost 100% charged or when the potential difference between the two series cells is at least 27V (13.5V/cell).

In the next section we will test the capabilities of a new balancing system.

III. TESTING WITH BATTERY BALANCER 2

The first balancer system has been replaced by another balancer, namely for commercial reason battery balancer 2, capable of balancing with a current up to 10A and with continuous operation. This equipment is shown in Fig.11. Also, in Figure 17 it is detailed that such a module is capable of balancing 4 series cells. For larger numbers than 4, such modules should be placed in series. This is the reason why the number of cells has been reduced from 6 to 4 to test the new equipment. Another important aspect is that this system works when the voltage potential between two batteries is higher than 24V. The choice of using a passive balancing system over an active one is motivated by costs and because of the large (10A) current that the passive structure can handle. Heat dissipation was not a problem as the devices do not show increased temperatures, balancing at 10A only in extreme voltage differences. Moreover, the balancing system is scalable to any number of series connected cells, so this gives a large flexibility when designing the battery pack. The charging time of the battery is not influenced by the balancing solution as that operates in parallel with the main battery supply.

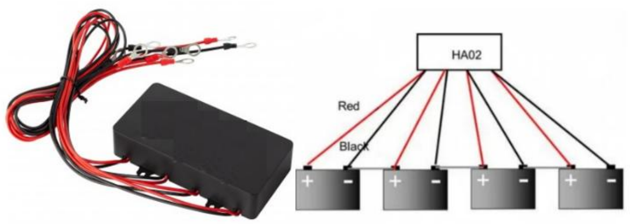

Fig. 17 Balancer 2 system

Therefore, the cell configuration was rebuilt with 4 elements in series, keeping the cell that showed the strongest imbalance out of the original 6. The first step for testing was to perform a load test in constant current and constant voltage in two steps.

The test results are shown in Figure 18. The first step, shown in Figure 18-left, demonstrates the charging process of initially unbalanced cells. A constant current of 10A is applied until the maximum voltage of a cell reaches the upper threshold of 14.5V, after which the total group voltage becomes the control reference for the constant voltage strategy. The current can be seen to gradually decrease to maintain the voltage at the reference value. The current being small, this time the balancing system able to direct it correctly to minimize the voltage difference on the cells. It can be seen in Figure 18-left how the difference decreases due to the balancing system and in approx. 4.5 hours, it reaches 0.25V. It can be also noted that some current ripples appear. The reason is the forced charging and thus the operation of the new balancing system.

The cells were left for 24h to be balanced by the new equipment and afterwards the charging process was resumed, detailed in Figure 19-right. It can be seen here how at start-up, a voltage difference occurs slightly over 0.5V, but is immediately rectified by the equipment then stabilizing around 0.1V. This confirms the proper functioning of the new balancing system.

Once these tests were completed, transient behavior were checked on real cycles. The first was the 500m run. This test was carried out for an 8h work schedule.

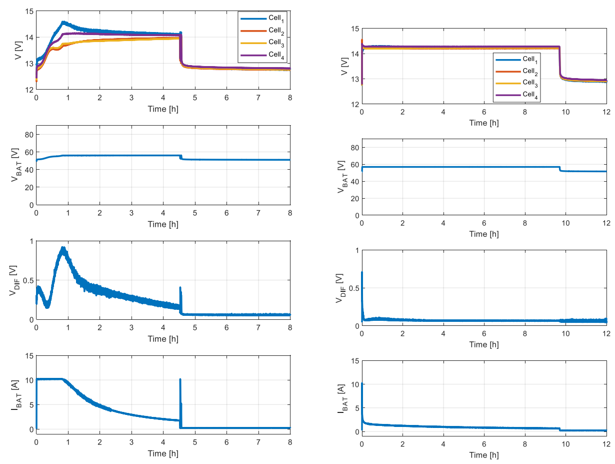

Fig. 18 Two-step balancing procedure

In Figure 19 -left shows the result of this study, and in Figure 19 -right, an area (between 4 and 5 hours of operation) has been enlarged for details. The battery system can cover a full 8h working program, and the maximum imbalance that occurs between cells is about 0.4V. The battery charge level decreases from 100% to about 40%, this is because the recovered energy is considered less than the consumed energy, i.e. the consumption time (raising the trolley), 3.4min, is longer than the recovery time (lowering the trolley) 2min. The break between them is 15min. These times were calculated based on the results from the Amesim simulation, where the funicular is built as a functional model with real data.

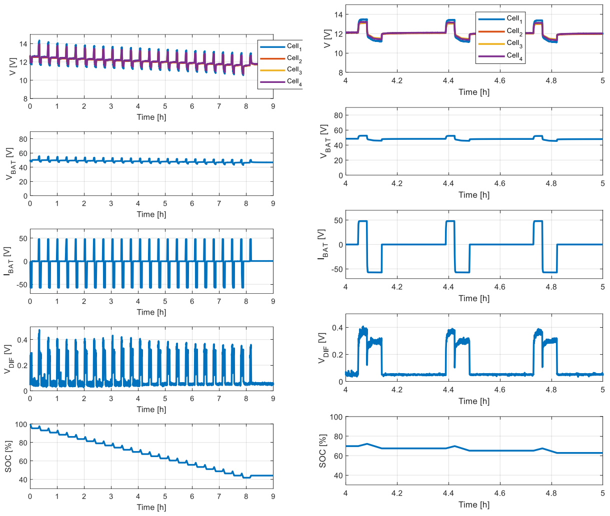

Fig. 19. Transient testing at 500m run

It is notable that throughout the entire operating period, the balancing system correctly manages the behavior of the cells, ensuring that they are balanced and that voltage differences are kept to very low values.

The next test that was performed was the 1000m route scenario, the same as the previous one, taken from the Amesim funicular model. As in the previous case, the testing was considered for an 8-hour work schedule. The ascent period of the trolley was 7.5min, i.e. a current consumption of 45A, and the descent lasted 4.2min with a 15min break in between (considered for charging) at a current consumption of 45A.

In Figure 20 we present the results of this test. The power system was able to serve 7.5h out of the 8h without any break considered. The cell voltage is well maintained in equilibrium, a more marked imbalance being marked at the end of the discharge process, where the SOC is in the 20% area. This is normal for any battery chemistry, including lead acid. Otherwise, the balancing system can withstand the balancing of voltages in such a way that the difference between them is kept somewhere below 0.5V.

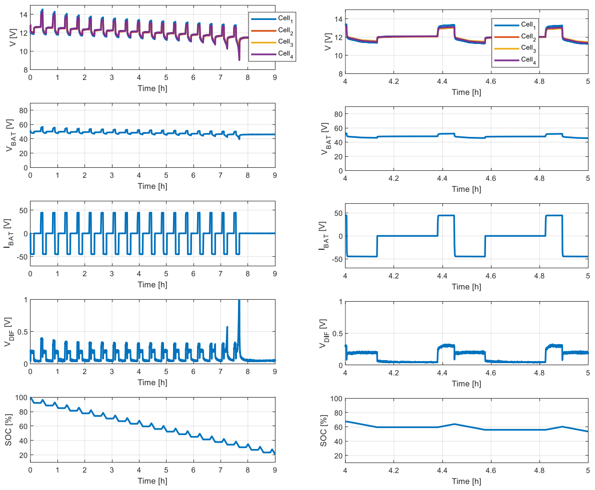

Fig. 20. Transient testing at 1000m run

The last two tests carried out were for the longest routes considered, namely 1500m and 2000m. These results are shown in Figure 21. Here it can be seen that, the routes being taken from the Amesim environment simulating the whole vehicle, at the 1500m route, the running time that the storage system supports is about 3.5h. Here the energy recovery period on the way down is about half of that on the way up.

Cell balance is ensured at a difference of less than 0.5V, the only exception being when an SOC below 40% is reached. At the 2000m run, the operating time is about 5h, longer than at the 1500m run because the charging period is approximately equal to the discharging period, but at a lower current. Thus, discharging is done at a current of approximately 52A and recovery at 48A. For this reason, the SOC decreases progressively. The cell balancing level is also kept below 0.5V, with the same assumption- the imbalance increases when SOC decreases a lot.

It should be noted that these paths were considered without optimal recovery control, i.e. at the same current each time, regardless of the current voltage or battery charge level. In the concluding section we will address a solution to extend the possibility of also serving the 1500m and 2000m runs for an 8h working schedule.

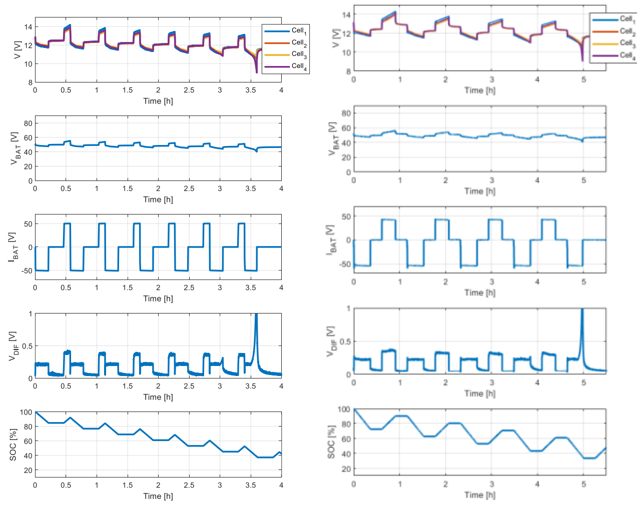

Fig. 21 Transient testing at 1500m (left) and 2000m (right)

Conclusions

The analysis of the battery storage behavior was dedicated exclusively to the funicular application as this was the single interest in the research project. Tests for other applications were not performed, however the authors trust for example, a grid tied storage system would behave also properly using these cells with their balancing units. The study carried out and detailed in the previous sections attests that the VRLA AGM lead acid battery storage system can serve the energy needs of the funicular system under development.

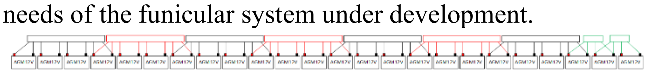

Fig. 22. Final structure of the battery system with balancing modules

Two voltage balancing solutions were tested, one of which was invalidated and the second validated as the one to be fitted to the final solution. At this level it should be noted that if the tests revealed an operation for only 4 cells, the extrapolation of the balancing system considered will be performed as shown in Figure 22. In this figure it is possible to distinguish the 24 cells connected in series respectively 7 balancing modules of 4 channels to which two dedicated balancing modules for 2 channels will be added. These last structures have the same behavior as the 4-channel ones but are dedicated for 2 cells in series. It can also be seen that, except for the first module, the rest are always referenced to the first cell of the previous 4 group. This ensures that all 24 cells will be maintained at the same voltage level, ensuring correct balance of the whole group. Regarding energy consumption and recovery, it has been observed from tests, especially at 1500m and 2000m that if recovery is done based on a simple, imposed current, the SOC of the battery drops and fails to cover the full 8-hour program. To expand the capacity of the storage system and to take advantage of it in the right way, the following energy recovery sequence is proposed:

- The recovery current should be the maximum current in the system, but no more than 70A, which is the capacity of one cell.
- the voltage of the group and the cells should always be monitored and the regenerative current calculated accordingly.

For the regenerative current the following rules need to be respected:

- if the voltage of a cell is close to 14.5V (the maximum safe voltage) we need to switch from maximum current control to maximum voltage control (the voltage level of the group obtained when any of the cells reaches 14.5V becomes the reference), keeping it constant and reducing the current for it (this regime corresponds to a 100% SOC);
- if the voltage of all cells is below 14.5V, the current shall be the maximum, but not more than 70A (the maximum current here is that which can be drained)
- the recovery current is 0 if the current value from the control regulator has fallen below 2A.

Energy consumption should be managed as follows:

- If the battery cell voltage is above 10V, the maximum current drained from the battery cells can be a maximum of 70A;
- if the voltage of any cell falls below 10V, the current drain must be interrupted and it is necessary to charge the battery at a constant current of 20A until any cell reaches 14,5V, at which point the constant voltage control is switched to constant voltage control until the current falls to a threshold of 2A.

Finaly, the main advantages of the system would be the low cost of the implementation, its reliability and the possibility of simple and fast replacement or fixing of the assemblies. However, the main disadvantage is the non-active and non-smart character of the balancing system, that nowadays is expected.

However, a compromise must be considered also regarding the application of storage, a funicular is isolated on its working land, generally with no internet access. Hence, the overall concept reaches the desired behavior in the budget considered.

Acknowledgment

This research has been supported by LEAP-RE MiDiNa project, grant N° 12, 01/04/2024

References

[1] Lates D., Inte R., Chirca M., Dranca M., Oprea C., (2023) Initial Evaluation of the Performances of a Sled-Type Forest Cableway. In: Moldovan, L., Gligor, A. (eds) *The 16th International Conference Interdisciplinarity in Engineering. Inter-Eng (2022).* Lecture Notes in Networks and Systems, vol 605. Springer, Cham.

[2] *IEEE Draft Recommended Practice for Maintenance, Testing, and Replacement of Valve-Regulated Lead-Acid (VRLA) Batteries for Stationary Applications, in IEEE P1188/D13*, February (2024), vol., no., pp.1-106, 17 April 2024.

[3] Kumar R., Shivam and Patil V., (2022) Performance Analysis of Energy Storage Unit with Lead-acid and Lithium Iron Phosphate Battery, *4th International Conference on Energy, Power and Environment (ICEPE)*, Shillong, India, 2022, pp. 1-6.

[4] Bhangu B. S., Bentley P., Stone D. A. and Bingham C. M., (2005) Nonlinear observers for predicting state-of-charge and state-of-health of lead-acid batteries for hybrid-electric vehicles, in *IEEE Transactions on Vehicular Technology*, vol. 54, no. 3, pp. 783-794.

[5] Zhang X., Li Z., Zhou D., and Chen M., (2023) State-of-Charge Estimation for Lead-Acid Battery Using Isolation Forest Algorithm and Long Short Term Memory Network With Attention Mechanism, in *IEEE Access*, vol. 11, pp. 49193-49204.

[6] Barsali S., and Ceraolo M., (2002) Dynamical models of lead-acid batteries: implementation issues, in *IEEE Transactions on Energy Conversion*, vol. 17, no. 1, pp. 16-23.

[7] Kutluay K., Cadirci Y., Ozkazanc Y. S., and Cadirci I., (2005) A new online state-of-charge estimation and monitoring system for sealed lead-acid batteries in Telecommunication power supplies, in *IEEE Transactions on Industrial Electronics*, vol. 52, no. 5, pp. 1315-1327.

[8] McKeon B. B., Furukawa J., and Fenstermacher S., (2014) Advanced Lead–Acid Batteries and the Development of Grid-Scale Energy Storage Systems, in *Proceedings of the IEEE*, vol. 102, no. 6, pp. 951-963.

[9] Azzollini I. A., (2018) *et al*., Lead-Acid Battery Modeling Over Full State of Charge and Discharge Range, in *IEEE Transactions on Power Systems*, vol. 33, no. 6, pp. 6422-6429.

[10] Setiawan D., Mahardiono N. A., and Purnama I., (2017) Time improvement technique of lead-acid battery balancing system, *2nd International Conference on Automation, Cognitive Science, Optics, Micro Electro-Mechanical System, and Information Technology (ICACOMIT)*, Jakarta, Indonesia, 2017, pp. 103-108.

[11] Chen S., Kang C., Zhang Z., and Zhu H., A (2016) Method for SOC estimation for lead-acid battery based on multi-model adaptive Extended Kalman Filtering estimation, *IECON 2016 - 42nd Annual Conference of the IEEE Industrial Electronics Society*, Florence, Italy, pp. 18-24.

[12] IEEE Draft Recommended Practice for Maintenance, Testing, and Replacement of Vented Lead-Acid Batteries for Stationary Applications, in *IEEE P450/D8, March 2017*, vol., no., pp.1-71, 9 June 2017.

[13] Upadhyay C., Patel H., and Mehta T., 2021 SoH Analysis of the Lead Acid (LA) Battery Using a Novel Vibration Tool, *1st International Conference on Power Electronics and Energy (ICPEE)*, Bhubaneswar, India, 2021, pp. 1-6.

[14] Cannone A. G., Salkind A. J., and Trumbore F. A., (1998) Comments on the evaluation of valve regulated lead-acid batteries (VRLA) under deep cycling regimes, *Thirteenth Annual Battery Conference on Applications and Advances. Proceedings of the Conference*, Long Beach, CA, USA, pp. 271-278.

[15] Hang W., Ya Z., Yan M., Xuejun S., Bo C., and Liuxu W., (2024) Research on SOC Estimation of Lead-Acid Batteries Based on ICS-PF, *IEEE 7th International Electrical and Energy Conference (CIEEC)*, Harbin, China, pp. 2728-2733.

[16] Shuo S., Jun-zhong S., Wei C., Yi-yang D., and Chao L., (2021) Research on an Algorithm for Prediction of Lead-Acid Battery Charging Time, *IEEE 4th International Conference on Electronics Technology (ICET)*, Chengdu, China, pp. 389-393.

[17] Degla A., Chikh M., Mzir M., and Belabed Y., (2022) The State Of Charge estimating methods for rechargeable Lead-acid batteries, *19th*

International Multi-Conference on Systems, Signals & Devices (SSD), Sétif, Algeria, pp. 496-502.

[18] M. P, S. S, G. U and G. R., (2023) Advanced lead acid battery care and monitoring system using cloud technology, *2nd International Conference on Advancements in Electrical, Electronics, Communication, Computing and Automation (ICAECA)*, Coimbatore, India, pp. 1-5.

[19] Suryoatmojo H., Anam S., Rahmawan Z., Asfani D. A., M. A. Faurahmansyah and Prabowo P., (2022) State of Charge (SOC) Estimation on Lead-Acid Batteries Using the Coulomb Counting Method, *10th International Conference on Smart Grid and Clean Energy Technologies (ICSGCE)*, Kuala Lumpur, Malaysia, pp. 78-84.

[20] Zhang S., and Xu Z., (2024) Research on The State Evaluation of Lead-acid Batteries Based on Fuzzy Comprehensive Evaluation Method, *IEEE 5th International Conference on Advanced Electrical and Energy Systems (AEES)*, Lanzhou, China, pp. 153-157.

[21] Bouharchouche A., Dali A., Kaabeche A., and Berkouk E. M., (2024) Experimental Parameter Identification of Lead-Acid Batteries using PSO Optimization, *2nd International Conference on Electrical Engineering and Automatic Control (ICEEAC)*, Setif, Algeria, pp. 1-4.

[22] Kumar C., Raj N., and Kumar P., (2024) Analysis of Charging and Discharging Characteristics Across Various Battery Types, *IEEE 1st International Conference on Green Industrial Electronics and Sustainable Technologies (GIEST)*, Imphal, India, pp. 1-6.

[23] Lavety S., Keshri R., Ghosh S., and Chaudhari M. A., (2021) Non-Linear Model and Parameter Extraction for Charge/Discharge Behavior of Valve Regulated Lead-Acid Battery, in *IEEE Transactions on Energy Conversion*, vol. 36, no. 4, pp. 2600-2611.

[24] Bolsi P. C., Prado E. O., Nazaré R. J., Sartori H. C. and Pinheiro J. R., (2023) Simple Method to Estimate Battery Lifetime of Lead-Acid and Lithium-Ion Batteries in Uninterruptible Power Supplies, *IEEE 8th Southern Power Electronics Conference and 17th Brazilian Power Electronics Conference (SPEC/COBEP)*, Florianopolis, Brazil, pp. 1-6.